Geo-Mar Lett (2016) 36:425–444
DOI 10.1007/s00367-016-0463-5

ORIGINAL

Geophysical evidence and inferred triggering factors of submarine landslides on the western continental margin of the Ulleung Basin, East Sea

Deniz Cukur[1] · Seong-Pil Kim[2] · Gee-Soo Kong[1] · Jang-Jun Bahk[1] · Senay Horozal[1] · In-Kwon Um[1] · Gwang-Soo Lee[1] · Tae-Soo Chang[3] · Hun-Jun Ha[4] · David Völker[5] · Jung-Ki Kim[1]

Received: 23 May 2016 / Accepted: 9 August 2016 / Published online: 17 August 2016

Abstract Submarine landslides form very complex depositional and erosional features on the seafloor, and their dynamics and triggering processes are yet to be understood completely. Numerous studies are being undertaken both because of the scientific significance but also for their potential harm to seafloor infrastructure and coastal areas. This study investigates the styles and causes of landsliding along the western margin of the Ulleung Basin in the East Sea, based on multiple sparker, subbottom profiler, multibeam echosounder and sediment core datasets collected in 2015. The bathymetric analyses indicate that the southern slope of the Ulleung Basin has experienced at least seven submarine failures. These failures left clear arcuate-shaped scarps that initiated at water depths of ~600 m. The observed headwall scarps have heights that exceed 60 m and appear to be the result of retrogressive-type failures. Seismic reflection data clearly image the basal sliding surface that is characterized by a prominent high-amplitude reflector. Chaotic-to-transparent seismic facies occur immediately downslope of the headwall scarps; these represent ~20 m thick landslide deposits. Gravity cores taken from areas adjacent to the scars suggest that these slides are older than ca. 97 ka. Interpretation of the present data shows that faults appear to cut recent sediments upslope of scarps, and that the slope may still be in an active phase of failure. Seismic data also image various overpressurized gases and/or gas fluids, as evidenced by the occurrence of pockmarks and seismic chimneys in upslope or adjacent areas of the scarps. Hence, earthquakes associated with tectonic activity and development of fluid overpressure may have acted as the main conditioning factor for destabilizing the slope sediments. Geotechnical stability analyses indicate that the sampled slope sediments are exceptionally stable under present-day conditions, even under seismic loading. This finding points to additional forces such as excess pore pressure caused by gas fluids at the times of slide emplacement.

✉ Deniz Cukur
dcukur@kigam.re.kr

[1] Petroleum and Marine Research Division, Korea Institute of Geoscience and Mineral Resources (KIGAM), Daejeon 305-350, Korea

[2] Korea Institute of Geoscience and Mineral Resources (KIGAM), Pohang 791-948, Korea

[3] Department of Ocean Science, Korea Maritime and Ocean University, Busan 49112, Korea

[4] Department of Ocean Sciences, Inha University, Incheon 402-751, Korea

[5] MARUM Center for Marine Environmental Sciences, University of Bremen, Bremen, Germany

Introduction

Submarine landslides are known to occur throughout the world marine margins and are the dominant sediment transport process from the continental margins to the deep sea (Locat and Lee 2002; Hutton and Syvitski 2004; Masson et al. 2006; Urgeles and Camerlenghi 2013). In some settings, up to 70% of the sedimentary column is reported to be composed of landslide deposits (Maslin et al. 2004; Newton et al. 2004). Landslides also represent a significant threat to offshore infrastructures, such as pipelines and telecommunication cables, and oil/gas platforms (Shipp et al. 2004; Camerlenghi et al. 2007; Yamada et al. 2012). The cost of damage to pipelines caused by submarine failures is estimated to be about US$ 400 million annually (Mosher et al. 2010). In

some cases, submarine landslides have generated tsunamis that have caused widespread damage as well as numerous fatalities in coastal communities (Tappin et al. 2001; Bondevik et al. 2005). Understanding the trigger mechanisms of submarine failures and submarine slope stability in general is of highest importance in terms of hazard mitigation for coastal areas, in particular as these areas are experiencing strong increases in population density globally. So far, the most likely preconditioning factors of submarine landslides are considered to be gas charging and gas hydrate dissociation (Sultan et al. 2004a; Mienert et al. 2005; Nixon and Grozic 2007), as well as sea-level changes, tidal changes, rapid sediment accumulation and under-consolidation, and erosional processes related to bottom currents (Kayen and Lee 1991; Hampton et al. 1996; Dan et al. 2007; Shanmugam 2009). Earthquakes are hypothesized to be one of the most important and frequent triggering mechanism in landslide initiation (Locat and Lee 2002; Sultan et al. 2004b; Masson et al. 2006; Leynaud et al. 2009; Völker et al. 2011). Individual mass failures can involve volumes as large as 20,000 km^3 over distances of more than 140 km (Hampton et al. 1996).

The seafloor of the western margin of the Ulleung Basin—focus of the present study—has slopes of up to 10° (Fig. 1). Many landslides initiated on these high-angle slopes. The margin is also characterized by low sedimentation even during sea-level lowstands, due to the absence of rivers along the adjacent coasts. Among researchers who investigated submarine landslides in the Ulleung Basin, Lee et al. (1996) and Horozal et al. (2016) reported numerous mass-wasting features on the entire margin primarily based on multi-channel seismic reflection profiles. According to Horozal et al. (2016), mass-transport deposits (MTDs) in the Ulleung Basin are about 600 m thick and thin towards the north to the base of the Korea Plateau. Lee et al. (1991) reported mass-wasting features in the north-western part of the basin, using high-resolution seismic reflection profiles. Chough et al. (1985) and Koo et al. (2014) mapped large-scale submarine gravity flows on the southern wall of the Ulleung Basin based on bathymetric data. These and other studies have placed important constraints on submarine sliding along the southern margin of the Ulleung Basin; many have postulated that earthquakes, gas charging and sea-level changes are the most probable causes for the initiation of these submarine landslides. Less has been published on submarine landslides along the western margin, a distinct geologic setting that has a different morphology (see below), structure, sediment thickness and lithology than the southern continental margin.

Within this context, the purpose of the present study is to document the distribution and characteristics of slides on the western margin of the Ulleung Basin, and attempt to understand the trigger mechanism(s). Sediment cores were taken adjacent to the headwall scarps in order to establish the ages of mass-transport deposits and to determine the sedimentological and geotechnical properties of slope sediments. Continuous coverage of the seafloor by multibeam echosounder data, along with sparker and subbottom chirp profiles as well as sediment cores offer a large-scale view of submarine slides on the western margin of the basin, enabling investigation of specific styles and processes of gravitational sliding.

Geological setting

The East Sea (Sea of Japan) consists of three basins: the Ulleung, the Japan and the Yamato basins (Fig. 1). The Ulleung Basin is a back-arc basin and occupies the south-western part of the East Sea. The basin was formed by a progressive drifting of the Japanese Arc south-eastwards accompanied by regional subsidence and tectonic movement during the late Oligocene and early Miocene (Ingle 1975).

The long axis of the Ulleung Basin trends approximately N–S and is about 230 km long (Fig. 1). To the west, the basin is bounded by its western margin. The shelf along the western margin is poorly developed, rarely exceeding 40 km in width, and includes a topographic high named the Hupo Bank (Fig. 1; Chough 1983). The Hupo Bank is about 80 km long and varies in width from less than 1 to 20 km. The bank shows a relatively flat top and lies between 10 and 200 m below sea level. Off the Hupo Bank to the east, the slope gradient gradually increases downslope to 10°. Three large faults characterize the western margin of the Ulleung Basin (Fig. 1), these being the Ulleung, Hupo and Yangsan faults. In the early Miocene, these faults activated concurrently, forming light-lateral strike-slip fault systems trending northeast (Yoon et al. 1997). The slope on the margin is covered with thin (<400 m) hemipelagic sediments (Horozal et al. 2016). The steep mid-to-lower slope is dominantly shaped by large-scale slope failures and associated mass-transport deposits (Chough et al. 1991). The slope lacks distinctive submarine canyons and fans, due to the absence of terrigenous input through large fluvial systems.

In sharp contrast to the western margin, a broad shelf (30–150 km wide) exists in the south and east. Here, the shelf is typically smooth and gently dipping northwards; the shelf break generally occurs at water depths between 300 and 400 m. Seismic reflection profiles revealed that sediment thickness on the margin reaches up to 3,000 m (Horozal et al. 2016). In addition, the presence of several submarine canyons along the southern margin of the Ulleung Basin suggests significant fluvial supply from southern sources (Park et al. 2015). The Oki Bank separates the Ulleung Basin from the Japan Basin. The rugged Korea Plateau is characterized by many ridges and troughs that rise up to 1,500 m above the basin floor.

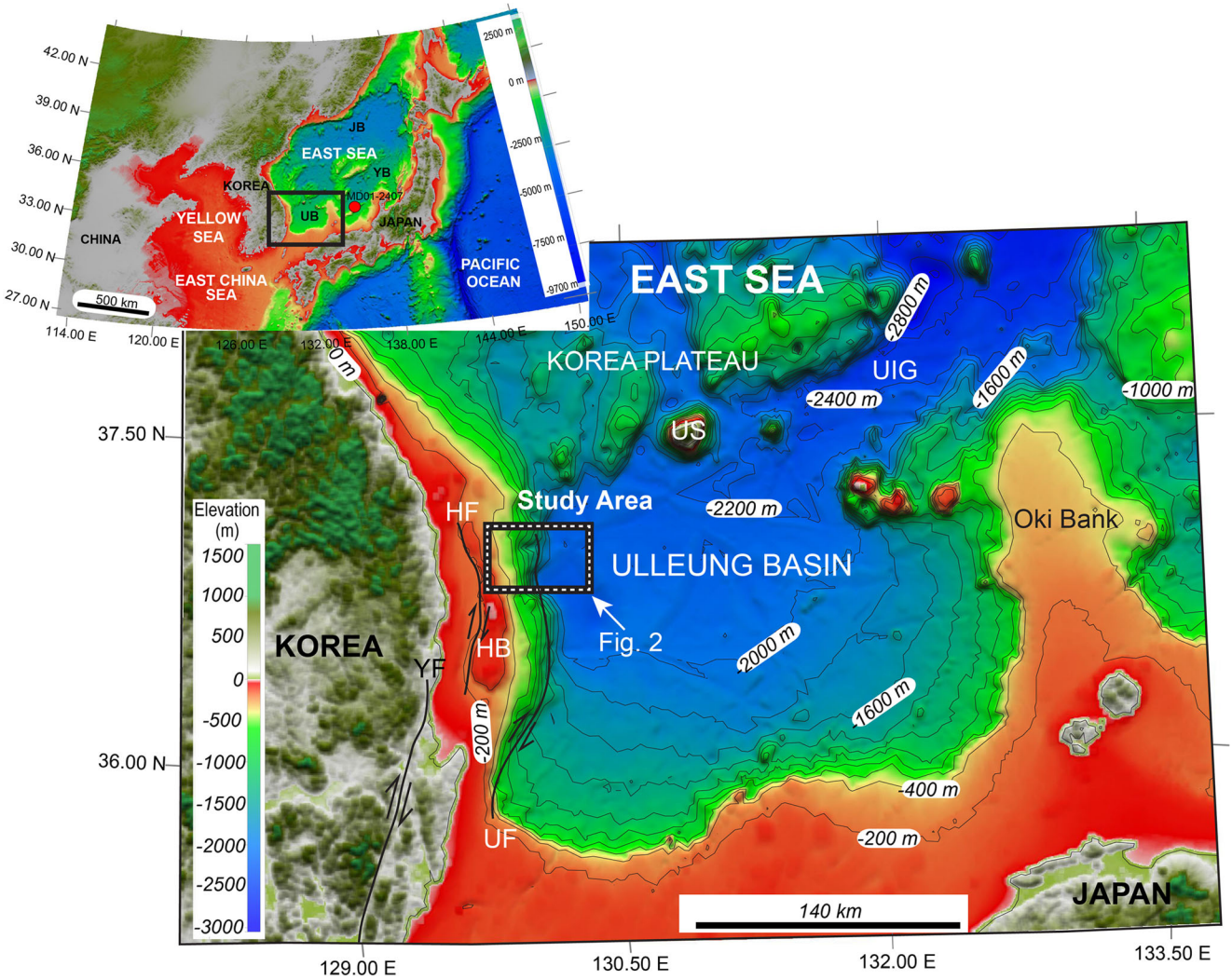

Fig. 1 Bathymetric map of the Ulleung Basin showing major tectonic elements as well as location of geophysical data acquired in 2015 (*rectangle* study area). *Red circle* Location of piston core MD01-2407 from Kido et al. (2007). *HF* Hupo Fault, *HB* Hupo Bank, *UF* Ulleung Fault, *YF* Yangsan Fault, *UIG* Ulleung Interplain Gap, *US* Ulleung Seamount

The Ulleung Seamount lies in the southern part of the basin and rises up to 900 m above the seafloor.

The basin floor that lies at water depths of 2,000 to 2,500 m is generally flat and progressively deepens to the north and northeast. The basin further connects to the Japan Basin by the Ulleung Interplain Gap (UIG), which is a narrow and long interbasin plain. Seismic reflection profiles suggest that the deep Ulleung Basin contains up to 5,000 m thick sediments; the acoustic basement in the southern basin lies below about 10 km (Chough 1983). According to findings of Lee and Suk (1998) based on regional seismic profiles, the latest Neogene–Quaternary sedimentary history of the basin includes two distinct phases: (2) the latest Neogene, characterized by widespread deposition of mass-transport deposits, and (2) the Pleistocene and Holocene, dominated by extensive turbidite and hemipelagic sedimentation.

Materials and methods

Data used in this study consist of (1) ~160 km long single-channel sparker profiles, (2) ~320 km long subbottom chirp profiles, (3) multibeam echosounder data and (4) five sediment cores (Fig. 2), collected in summer 2015 within the frame of the Korean Geological Mapping project. The sparker, chirp and multibeam data were acquired simultaneously from aboard the R/V Tamhae II. The sparker data were collected using a 2,000 J energy source and a short, single-channel hydrophane array. The centre frequency for the sparker system was ~250 Hz, with 4 s shot interval and 3.8 s recording length. Data processing included band-pass filter, deconvolution and surface-related multiple attenuation. The subbottom chirp data were collected by means of a BATHY 2010 system. Signal penetration was up to 40 m with a vertical resolution of 10 cm. The multibeam echosounder data were recorded using a

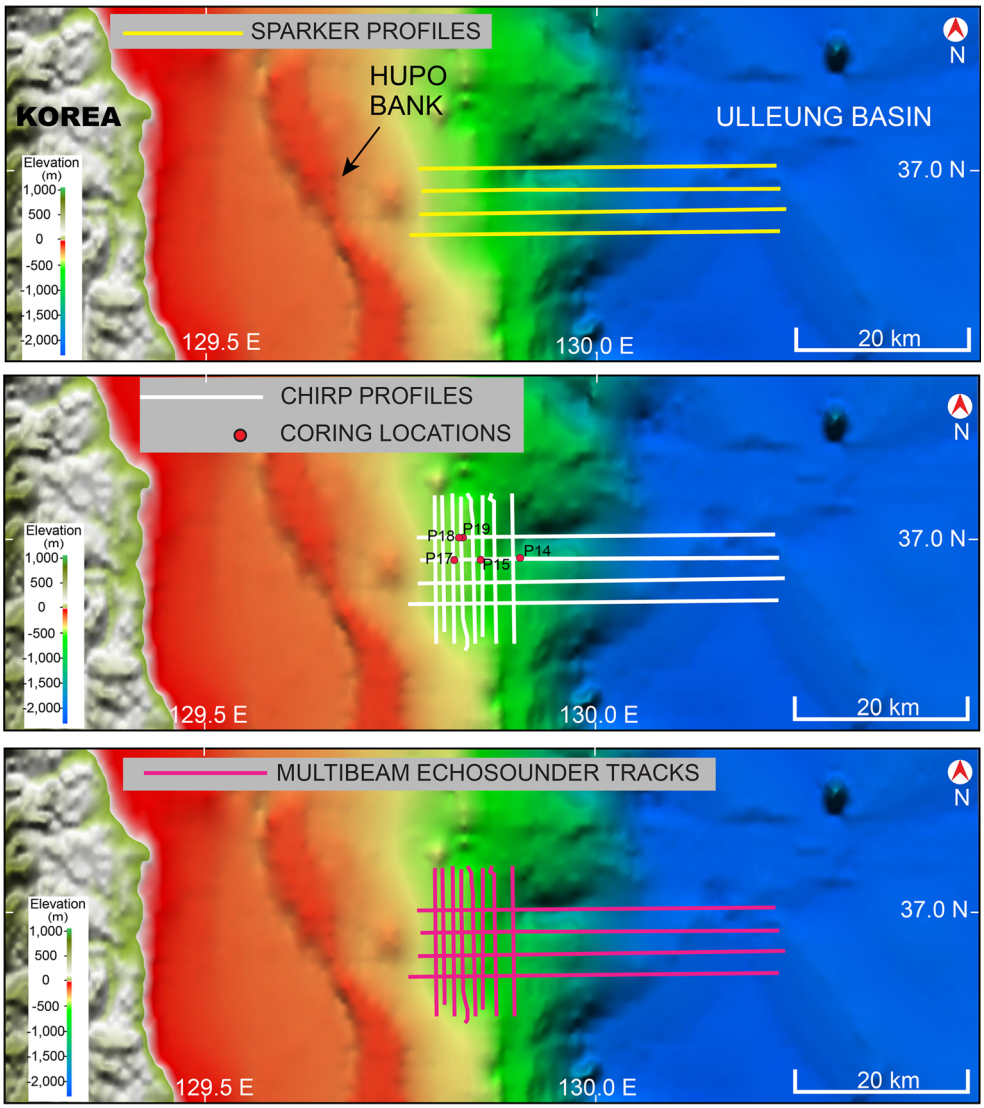

Fig. 2 Bathymetric maps showing the location of geophysical data as well as sediment cores acquired in 2015 ("Geological Mapping of the Korean Seas" project)

KONGSBERG EM 302 multibeam system, a swath sounder operating at a frequency of 30 kHz with up to 432 soundings per swath. Post-processing of the data was performed using CARIS HIPS & SIPS hydrographic cleaning system software. The IHS Kingdom Suite software served for data interpretation and mapping.

Five sediment cores (up to 5 m) were taken along the slope to determine sedimentary facies and geotechnical properties (Fig. 2). X-radiographs of 1 cm thick slabs (30 cm long) were taken from the one half of the split cores. Water content, grain density and bulk density were measured following a slightly modified method of the Ocean Drilling Program (Blum 1997) for samples collected with a nominal interval of 10 cm. After the moisture and density measurements, the remaining samples were taken for grain-size analysis using a laser-scattering particle analyzer (Microtrac S3500). Digital images were acquired by means of a line scan camera, and lightness (L*) profiles were deduced from the images of the other half of the split core surfaces. Miniature vane shear tests were conducted to measure undrained shear strength at 10 cm interval.

Determination of the stability of slope sediments is based on calculation of the factor of safety (FOS), assuming either static loads (FOS_{static}) or seismic loading (FOS_{eq}) as the driving forces of mobilization. If FOS >1, the sediments are assumed to be stable. A slope is unstable when the FOS ≤1 (Morgenstern and Price 1965). In the calculation of FOS_{static}, the undrained shear strength (S_u) of the sediment column at a given depth z (representing the resisting force) is balanced against the driving forces of a slide along a slope-parallel failure plane:

$$FOS_{static} = \frac{S_u}{\gamma' z \sin\theta \cos\theta} (\text{undrained}) \quad (1)$$

where θ is the slope angle of the scar area (about 2.4°) and γ' is the buoyant weight (density difference between solid and water multiplied with g) of the material that is likely to fail

(Morgenstern 1967). For the calculation of the factor of safety against seismic loading FOS_{eq} under undrained conditions, the pseudostatic formula of ten Brink et al. (2009) was used:

$$FOS_{eq} = \frac{S_u}{\gamma' z\left[\sin\theta\cos\theta + k_e\left(\frac{\gamma}{\gamma'}\right)\cos^2\theta\right]} \text{(undrained earthquake)} \quad (2)$$

where θ is the slope angle, k_e is the cyclic load of an earthquake represented by a constant horizontal acceleration (expressed as a percent of gravity) required to cause failure, γ is unit weight of the bulk sample, and γ' is the buoyant weight (density difference between solid and water multiplied by g) of the material that is likely to fail.

Results

Multibeam bathymetric data

Bathymetric data collected along the western margin of the Ulleung Basin span a depth range between 500 and 2,200 m (Fig. 3). The bathymetric analyses indicate a complex morphology of slides with at least seven arcuate-shaped headwall scars (Fig. 3b). Such geomorphology is typical for retrogressive slab-type failures (Krastel et al. 2012).

The headwall scars reach heights of about 60 m and are typically found at water depths of 600 m (Fig. 4a, b). Within the headwall scars, slope gradients are as steep as 30° (Fig. 4a). The total evacuated area is about 120 km^2 and the estimated volume of displaced sediments is about 6 km^3. The upper slope directly above the scars has an angle of 2.4° (Fig. 4c). The middle slope has a gradient of 4.5° down to 1,200 m, and the lower slope has a gradient of 10° down to 2,150 m where it merges into the flat basin floor. The lower slope has steeper slopes than the upper and middle slopes, owing to its location on the western side of the Ulleung Fault.

Sparker profiles

On four E–W trending sparker profiles covering the upper shelf and slope regions down to the base of the slope and basin floor, several landslide features were clearly identified (Fig. 5). The sparker profile presented in Fig. 5a shows an area of rather disturbed reflections east of a morphological step representing a headwall scarp. The chaotic-to-transparent seismic facies immediately downslope of this morphological step is typical for mass-transport deposits (MTDs; Krastel et al. 2006; Strozyk et al. 2010), distinctly contrasting from the undisturbed, well-stratified slope sediments. The deeper underlying reflections have the normal, parallel, flat-lying appearance characteristic of undisturbed slope sediments.

Several slide blocks occur downslope of scarps at water depths between 700 and 1,700 m (Fig. 5a, b). They are characterized by a hummocky surface with internal transparency. With a relief in the order of 5–10 m, individual slide bodies reach up to 40 m in thickness (assuming a velocity of 1,600 m/s) and 0.6 km in length. Some of these slides and slumps reach the base-of-slope regions, forming lens-shaped depositional bodies (in cross section) with a maximum thickness of 40 m (Fig. 5c). The internal structure of the lens-shaped bodies shows transparent seismic facies. The lack of internal sedimentary structure within MTDs is caused by sediment flow and mixing during downslope displacement, which destroys internal structure and gives MTDs their characteristic acoustic transparency in sparker profiles. The MTDs appear to have travelled over a distance of 30 km downslope. Beyond the toe of the slide, the basin is characterized by parallel seismic reflections (Fig. 5c).

Figure 6 depicts another large slide deposit along the continental slope in the southern part of the study area, with a prominent headwall of nearly 40 m height (Fig. 6b). A chaotic seismic unit is imaged immediately downslope of the failure scarp; the seafloor is characterized by a hummocky morphology. A closer look at the sparker data on Fig. 6b reveals some internal stratification of individual blocks, which can be explained by relatively intact slide blocks that have not moved very far. The base of the slide is marked by a prominent continuous high-amplitude reflector, which represents the glide plane (Fig. 6b). The glide plane reflector appears to be covered by 60 m of undisturbed slope sediments upslope of the headwall scarps (assuming a velocity of 1,600 m/s). This reflector, as well as others below, can be traced laterally from beneath the slide into the adjacent continental slope in several places, confirming that these buried sediments have not been displaced. The chaotic-to-transparent facies of the slide deposit forms a wedge-shaped body thinning downslope. About 25 km downslope of the headwall in the base-of-slope region, the MTDs thicken significantly to almost ~20 m (Fig. 6c); this region probably represents the main depositional area of the slides. At the toe of the slides towards the basin floor, seismic reflections become continuous and well stratified. An “erosional step” in the surface of underlying sediments is also evident.

Also evident are several seismic chimneys on the sparker profiles, which would be caused by vertical migration of gas (Fig. 6b; cf. Horozal et al. 2009; Hustoft et al. 2010). These chimneys appear to root from deeper sedimentary strata and terminate at different stratigraphic levels.

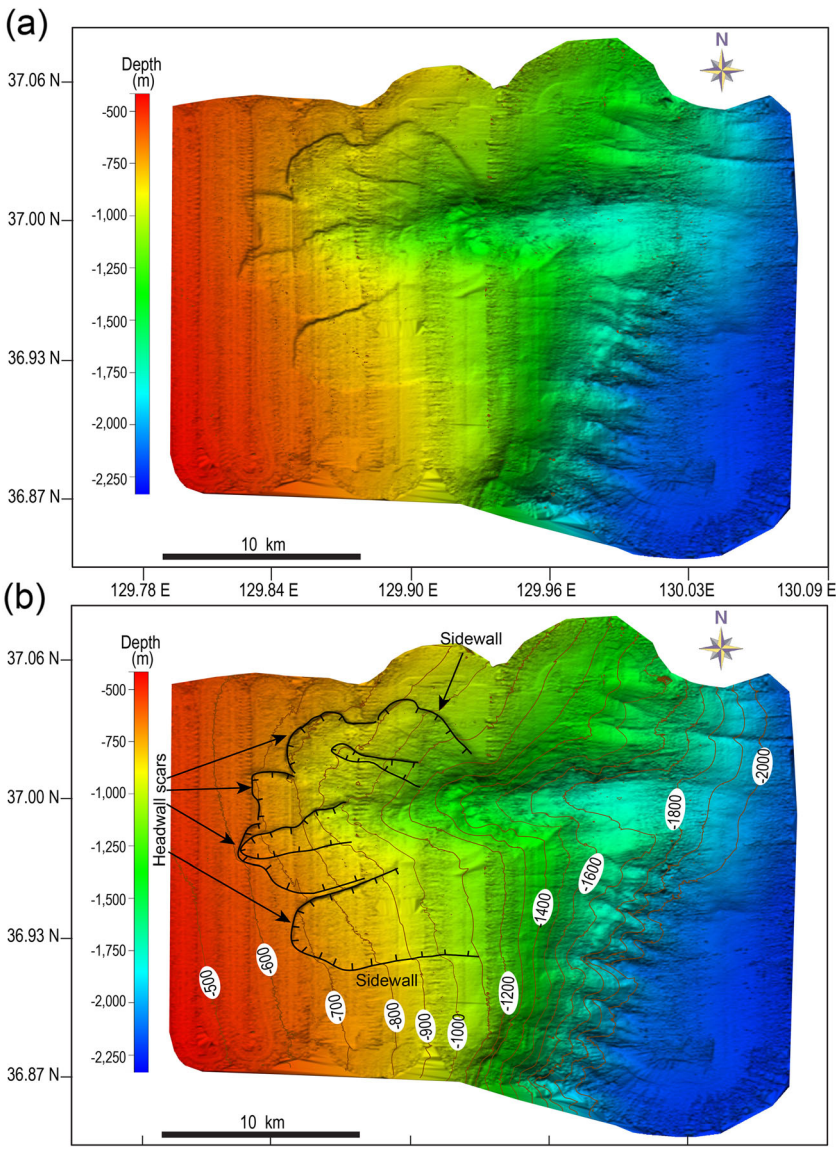

Fig. 3 **a** Bathymetric map along the western margin of the Ulleung Basin at water depths of 500–2,200 m. **b** Bathymetric analyses indicating a complex morphology of slides with multiple arcuate-shaped headwall scars and at least seven failures. The step-like morphology of these slides suggests retrogressive failure

Subbottom chirp profiles

Two subbottom profiles traversing morphological steps in the slide area clearly illustrate MTDs beneath the headwall scarps (Fig. 7), associated with chaotic-to-transparent acoustic facies. The eastern parts of the scarps are characterized by a hummocky seafloor caused by MTDs, whereas the western parts have a smooth seafloor representing undisturbed slope sediments. A thin sedimentary drape is evident on top of the MTDs, its thickness being about 6 m (assuming a velocity of 1,600 m/s). There is an apparent lack of sediment drape on the headwall scarp. The profile in Fig. 7a also shows various slide blocks downslope of the headwall scarp; a recent slide can be seen in a close-up section in Fig. 7a, which is slightly deformed internally.

Two chirp profiles crossing the study area in a N–S direction (Fig. 8) reveal numerous faults in close vicinity of headwall scarps, some of which extend to the seafloor. Some of these faults show characteristics of reverse faults. In addition, there is evidence of truncation of well-stratified sediments along the sidewalls of scarps.

Another chirp profile reveals a V-shaped seafloor depression on the upper shelf (Fig. 9a), which is nearly 5 m deep and 150 m wide. This feature is interpreted as a pockmark (cf. Hovland et al. 2002). Their occurrence is confined to areas upslope of the scarps (Fig. 9b), where the sediments are undisturbed. The available data do not enable to determine if gas seepage is still active. A buried pockmark can be seen at a depth of about 0.83 s TWT (Fig. 9a).

Sedimentary characteristics and physical properties

Five sediment cores were collected along the slope, two (P17 and P18) from the undisturbed slope above the

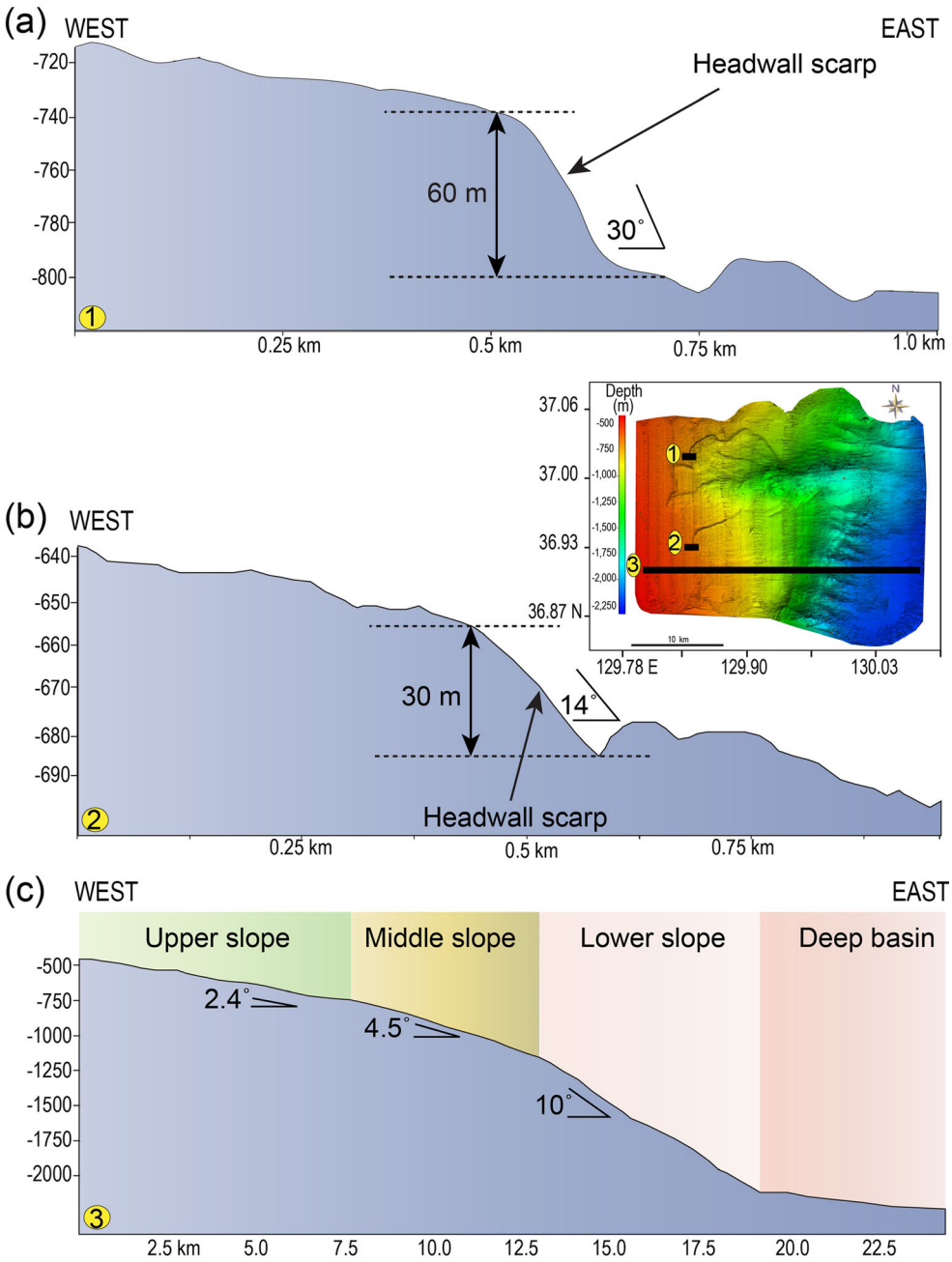

Fig. 4 **a**, **b** Bathymetric profiles 1 and 2 across headwall scars, revealing heights ranging from 30 to 60 m and slope gradients as steep as 30°. **c** Bathymetric profile 3 across the slope, with gradients ranging from 2.4° to 10°

headwall scarps, the others (P14, P15 and P19) from the proximal and distal parts of evacuated sediment masses (Fig. 10). The core sediments mostly consist of sandy mud and mud with an average mean grain size of 6.2 (Table 1), except for a few intercalated tephra layers of scattered pumice lapilli (Fig. 11). They are either bioturbated or crudely laminated with cyclic changes in sediment lightness. The bioturbated sandy mud or mud (BM) facies is dominant and is characterized by mottling and pyrite filaments of variously shaped burrows (Fig. 11). The crudely laminated sandy mud or mud (CLM) facies is characterized by continuous or discontinuous horizontal laminae that often include abundant foraminifera. The facies units are 2 to 28 cm thick and alternate with the BM facies with sharp lower and gradational upper boundaries (Fig. 11). The BM and CLM facies are equivalent to those described by Bahk et al. (2000) in the Ulleung Basin, interpreted as having been formed by hemipelagic settling under well- to poorly oxygenated bottom-water conditions controlling the degree of bioturbation by benthic fauna. Although the present study aimed at recovering MTDs from slope failures in cores P14, P15 and P19, none of these recovered MTDs as the corer did not penetrate below the hemipelagic drape.

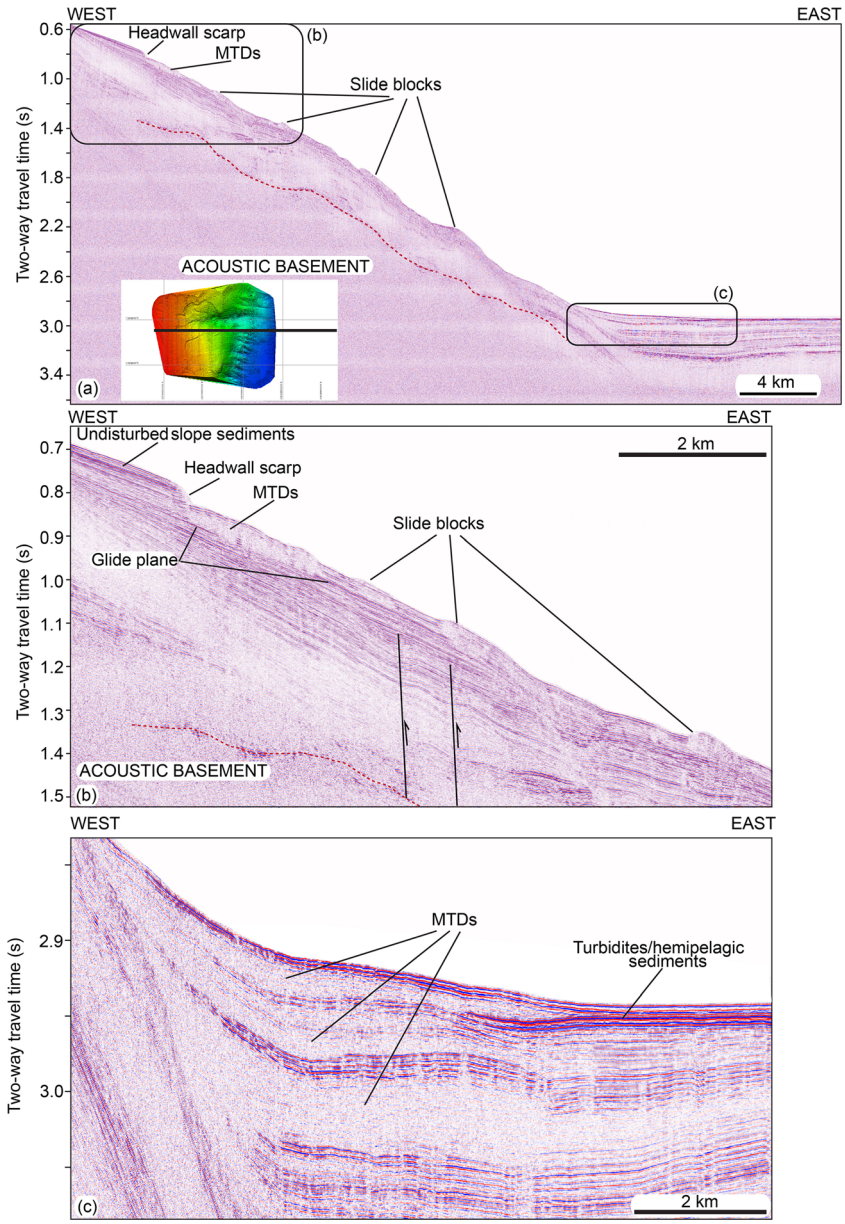

Fig. 5 **a** Representative sparker profile showing a headwall scarp, MTDs and slide blocks across the western margin of the Ulleung Basin. **b** Chaotic facies downslope of the scarp represent MTDs. Sediments on the western side of the scarp are well stratified, indicating that they are not affected by the sliding event. Various slide blocks occur downslope of the scarp. **c** Lens-shaped MTDs in the base-of-slope region, grading into well-stratified turbiditic sediments at their distal edge

Profiles of physical properties show typical variations with core depth (Figs. 12 and 13). On the undisturbed seafloor, water content, porosity, wet bulk density and grain density are earmarked by abrupt changes at a depth of 80 cm in core P17 and 100 cm in core P18 (Fig. 12). Spikes in the profiles coincide well with intervals over which the sediment texture changes significantly. Shear strength (average 7 kPa) steadily increases with depth, reaching 10 kPa at depths of 200 cm. In contrast to the upslope sediments, the surficial sediments downslope of scarps overlying the slide deposits have high shear strengths of up to 30 kPa (average 8 kPa, Table 1, Fig. 13). Similar to the sediments upslope of the scarps, the water content, porosity, wet bulk density and grain density show abrupt peaks over specific depth intervals, suggesting facies changes (Fig. 13). This variability is revealed particularly well in the profiles of water content and wet bulk density.

Age model and sedimentation rate

Cyclic variations of dark- and light-coloured sediments in the Quaternary succession of the East Sea are known to reflect orbital and millennial-scale changes in palaeoceanographic conditions, and have been widely used to establish high-resolution age models of the sediments (e.g. Kido et al. 2007; Khim et al. 2008; Bae et al. 2014). An age model for this study was established by correlating sediment lightness (L*) variations in core MD01-2407 (see Fig. 1 for location; Kido et al. 2007) with those in core P14, which seems to have

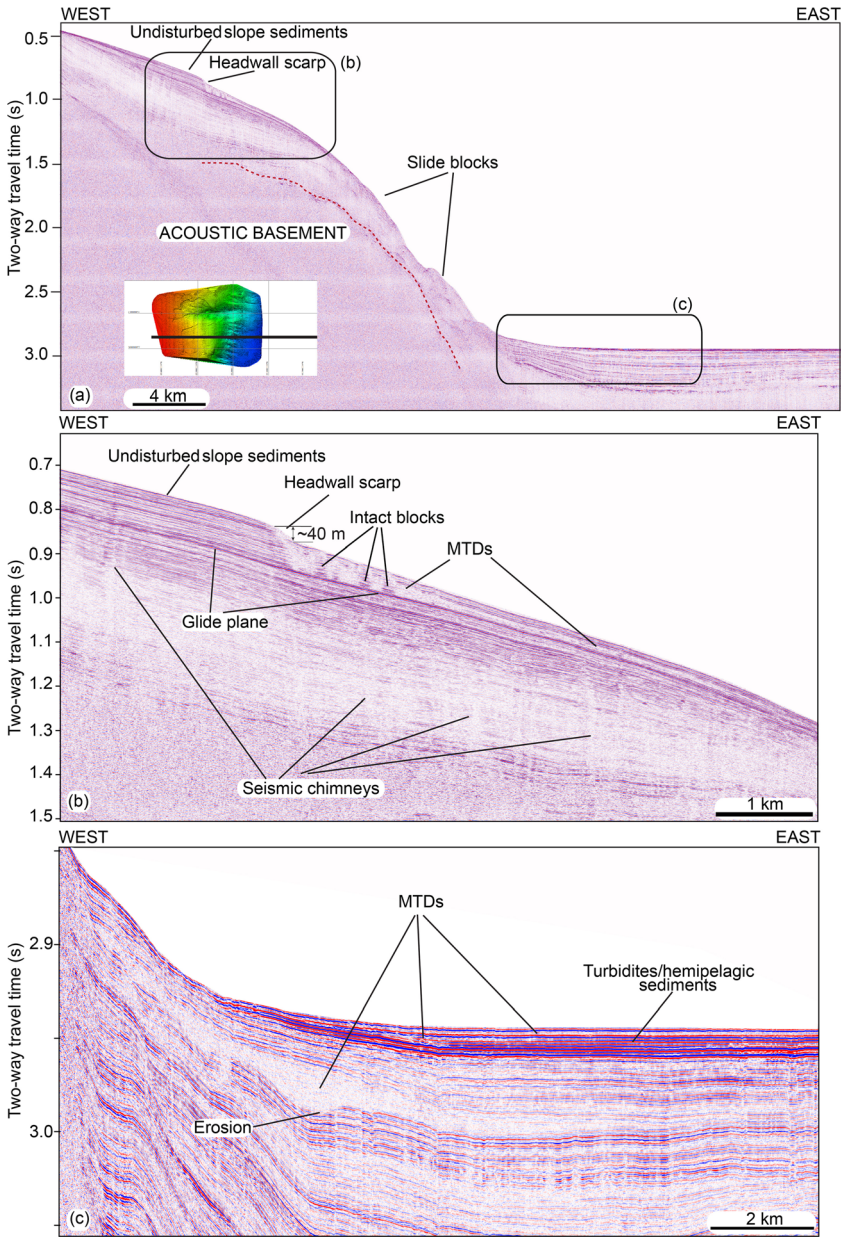

Fig. 6 **a** Representative sparker profile crossing a headwall scarp (~40 m high) in the southern part of the study area. **b** MTDs occur immediately below the scar and are characterized by chaotic-to-transparent seismic reflections. The base of MTDs is marked by a high-amplitude reflector, which may represent a glide plane. **c** Some of these slides and slumps reach the base-of-slope region, forming lens-shaped depositional bodies

retrieved the longest record (Fig. 14a). The occurrence of tephra layers of known age—U-Oki (ca. 10.7 ka) and SKP-II (60–61 ka), consisting of scattered pumice lapilli—confirms that the age correlation is valid (cf. Chun et al. 2007). Depth-to-age conversion of the other core sediments is based on correlations of L*, tephra layers and CLM facies between the cores (Fig. 14b).

The established age model indicates that core P14 from the deepest water depth (1,040 m) dates back to 97.4 ka. Therefore, the MTD overlain by this hemipelagic sediment is older than this age (Fig. 14a, b). The cores within the proximal parts of the slide scar have higher sedimentation rates (P15: 9.2 and P19: 6.8 cm/1,000 years) than those from the undisturbed upslope sector (P17: 3.2 and P18: 6 cm/1,000 years; Fig. 14c). All the cores tend to show much higher sedimentation rates during the Holocene.

Slope stability analyses

Slope stability was analyzed for two sediment cores (P17 and P18; Fig. 15) collected in the unfailed slope regions immediately above the headwall scarps. Calculation of FOS_{static} (undrained; Fig. 15a) yields a minimum value of about 9 for a given slope gradient of 2.4 at 600 m water depth.

Figure 15b reports $FOS_{seismic}$ in response to an earthquake creating a pseudostatic acceleration of k_e*g. When the slope

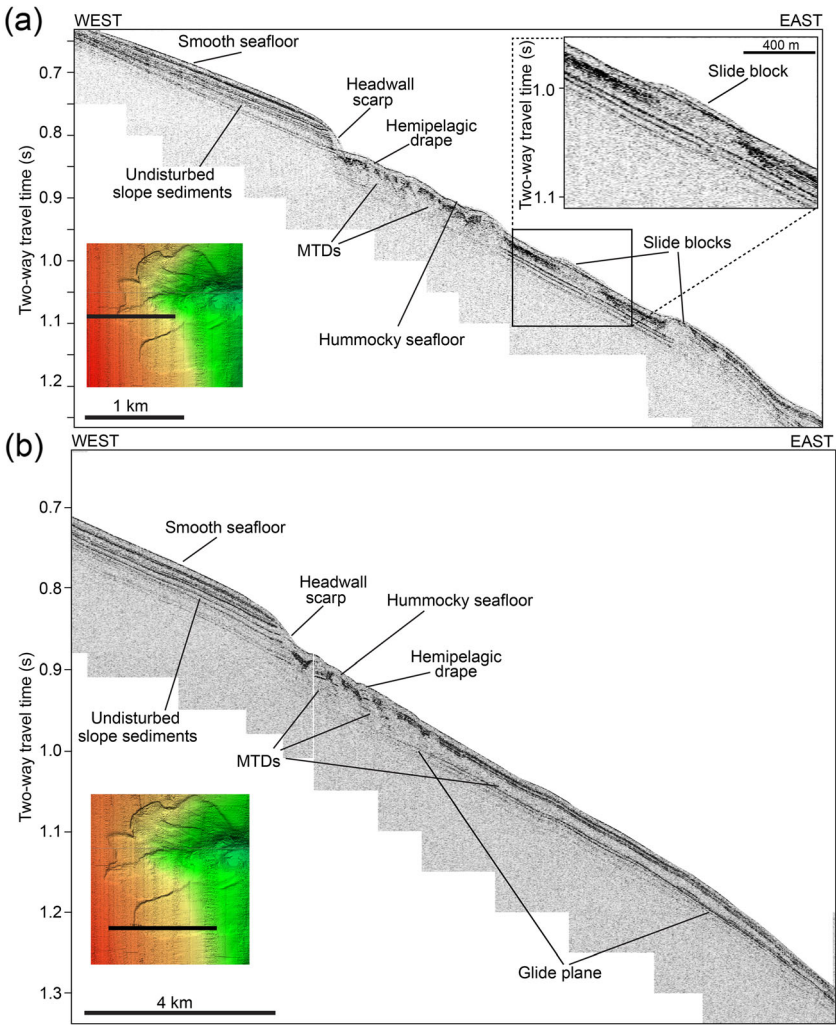

Fig. 7 **a**, **b** Subbottom chirp profiles clearly show landslide scars and associated deposits across the slope. At the foot of the scarp, MTDs are covered by a ~6 m thick sedimentary drape

undergoes an acceleration of k_e=0.1, which is the average estimated value for the western slope of the Ulleung Basin with a corresponding earthquake intensity of Mw=5 (Chough and Lee 1987), $FOS_{seismic}$ drops to a minimum value of 10 at a depth of 3 m. Increasing the effect of a hypothetical earthquake (by increasing k_e) does decrease the FOS in comparison to the static case; this would, however, need unrealistically high k_e (that is, unrealistically strong earthquakes in close vicinity) to bring it down to 1 (to fail the slope) at any depth. Nevertheless, the effects of an earthquake may be amplified by the local soil conditions (Baraza et al. 1992).

Discussion

Based on the newly collected data described above, it is evident that submarine failures are common along the western margin of the Ulleung Basin. The nature of the failures varies and has produced scarps on the upper slopes, slide blocks on the middle to lower slopes, stacked MTDs at the base of the slope, and turbidity currents on the deep basin floor (Fig. 16). The transition of slide deposits into turbidites and hemipelagic sediments is reflected on the sparker profiles by the occurrence of well-stratified seismic reflections at their distal edge. It might well be that a turbulent cloud following a slide is transported further downslope and deposited in the deep basin.

A similar zonation of slide masses has been reported for other parts of the Ulleung Basin. Along the south-eastern margin, for example, sediment failures are found on the upper slopes, subsequent sliding and slumping on the upper to middle slopes, debris flows at the base of slopes, and the development of turbidity currents in the central part of the basin (Chough et al. 1985). Slides with scarps about 200 m high and downslope debris flows are described by Koo et al. (2014) for the southern margin of the Ulleung Basin. They proposed that earthquakes might be a significant factor affecting sediment instability in this sector. Much of the seismic evidence for offshore debris flows around the Ulleung Basin has been

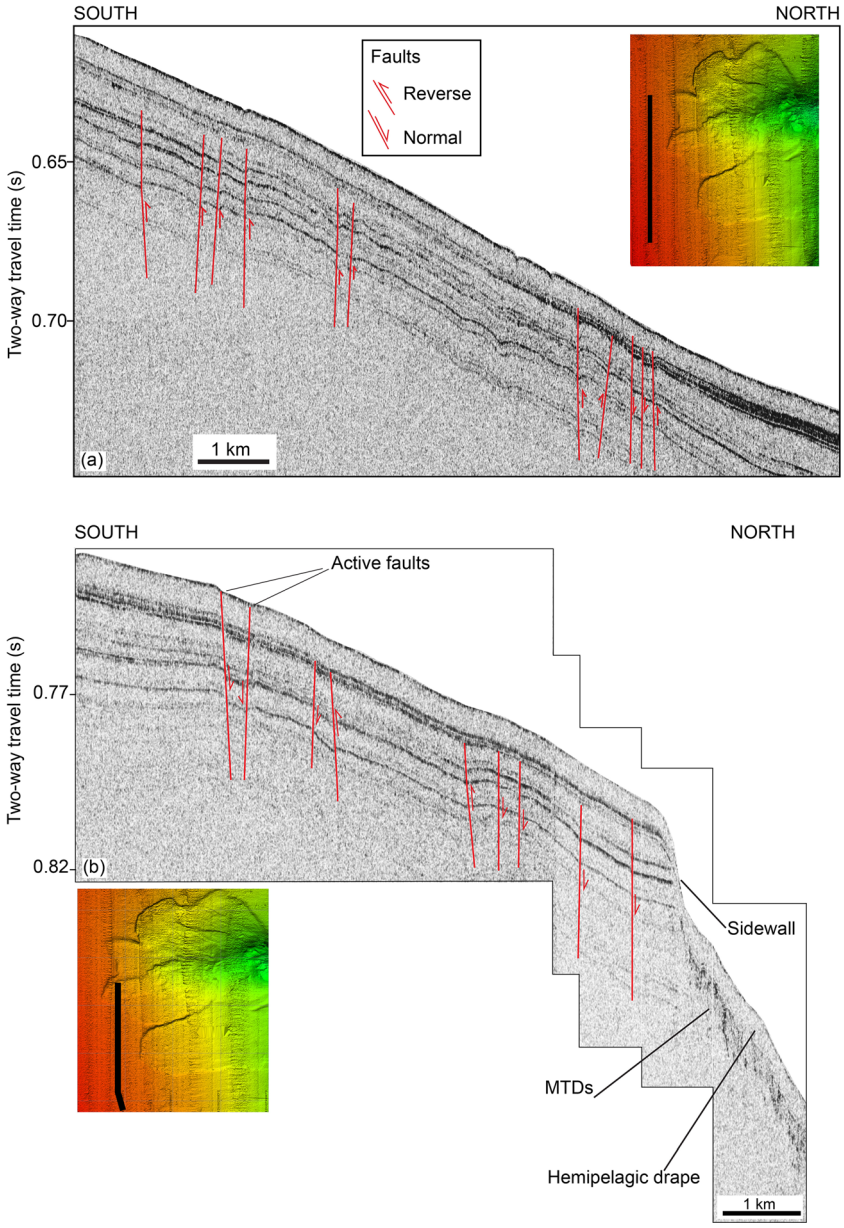

Fig. 8 **a**, **b** Subbottom chirp profiles showing numerous faults in the upslope areas of a headwall scarp. Some appear to offset the seafloor, suggesting recent activity

evaluated by Horozal et al. (2016), including an overview of submarine failures on the southern margin, the areal extent and volume of submarine debris flow deposits, and the inferred ages and a comparison with known landslides. Tectonic activity, high sedimentation rates and gas hydrate dissociation were suggested as possible triggers for these slides. Horozal et al. (2016) also concluded that the largest submarine slides (up to ~550 km^3) occurred on the southern margin of the Ulleung Basin, an area where thick terrigenous sediments were deposited during lowstands (Chough et al. 1985). The volume of displaced sediments (~6 km^3) in the present study area is rather small compared to the large-scale slides on the southern margin (10–550 km^3; Horozal et al. 2016), which can be explained by low sedimentation rates along the western margin.

Seismic data show that glide planes are characterized by prominent high-amplitude reflections (Figs. 5b and 6b). The high-amplitude character of these surfaces can be explained by several factors. The significant acoustic impedance contrast may result from an abrupt lithologic or diagenetic change along this boundary. Another explanation could be that the passage of the flow over the top of the surface may have compacted it, thereby increasing its density and consequently its impedance. Alternatively, the slide may have left rubble on the surface that, although smaller than the vertical resolution, creates substantial sound diffraction resulting in strong

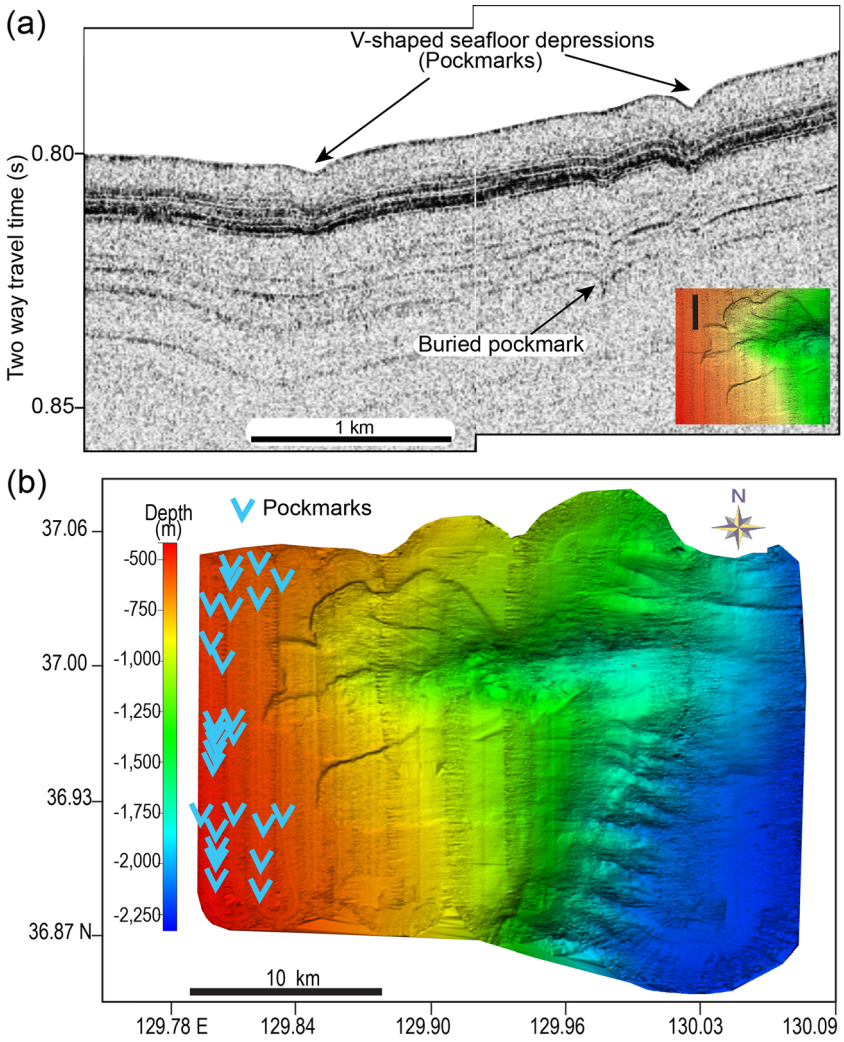

Fig. 9 **a** Subbottom chirp profile crossing upslope areas of scars, showing V-shaped pockmarks on the seafloor and a buried pockmark. **b** Distribution of pockmarks concentrated in upslope regions of headwall scarps

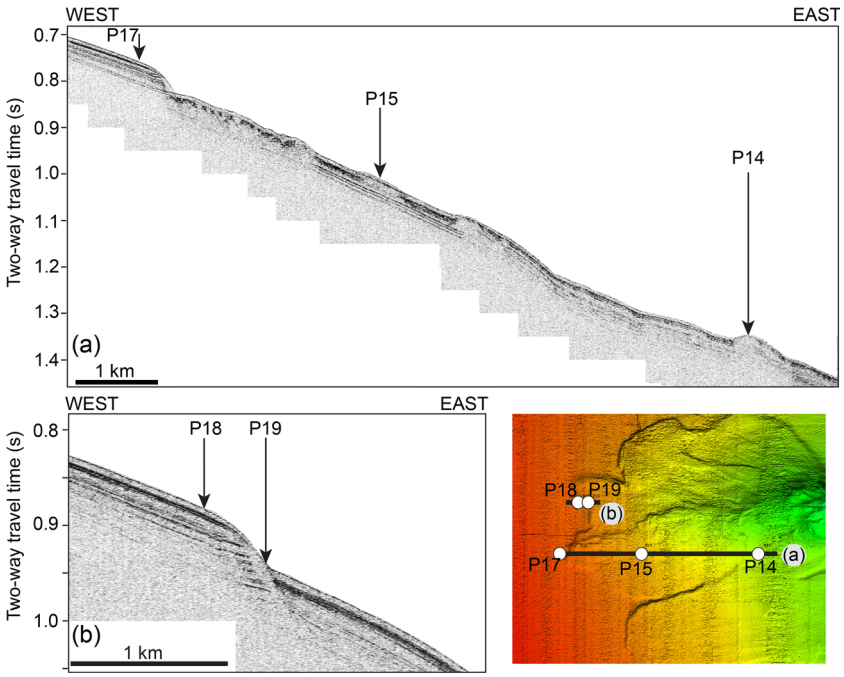

Fig. 10 Subbottom chirp profiles together with bathymetric map of piston core locations that have been projected onto the profiles to show their morphology and stratigraphic setting

Table 1 Average textural and physical properties of sediment cores from the western slope of the Ulleung Basin

Core ID	Water depth (m)	Mean grain size (ϕ)	Sand (%)	Silt	Clay	Water content	Porosity	Wet bulk density (g/cm^3)	Grain density	Shear strength (kPa)
P14	1,040	6.4	7.0	85.0	8.0	54.0	74.0	1.40	2.5	12.0
P15	790	6.2	13.0	79.0	8.0	55.0	75.0	1.40	2.4	10.0
P17	590	6.15	11.0	81.0	7.0	52.0	73.0	1.42	2.5	7.0
P18	640	6.14	10.0	85.0	6.0	53.0	73.0	1.44	2.6	6.8
P19	690	6.23	11.0	81.0	7.0	57.0	77.0	1.40	2.6	7.5

reflection. As the existing data cannot confirm the nature of the plane, further studies such as deep drilling into the glide plane are needed.

The formation of erosional steps in buried slides suggests that the flow was capable of scouring the surface to depths of a few meters (<5 m) at the base of slope (Fig. 6c). This may further imply that the flow became more dynamic and erosional while passing the base of the slope. Also, the sediment thickness of this buried slide appears to be higher than the younger slide deposits, suggesting that it was a rather large slide. Similar erosional features have been identified in the base-of-slope regions on the southern margin of the Ulleung Basin, and have been attributed to an abrupt change in slope gradients (Lee et al. 1999).

Subbottom chirp profiles show lack of sediment drape on the headwall scarps, which may suggest erosion related to bottom currents. This is reflected in the sediment cores by varying sedimentation rates within and outside of the headwall; thick sediments are found along the floor of the headwall whereas thin sediments occur outside of the headwall scarps (see Fig. 14b, cores P18 and P19). These varying accumulation rates suggest that bottom currents could play a significant role in the deposition and re-deposition of sediments in this area.

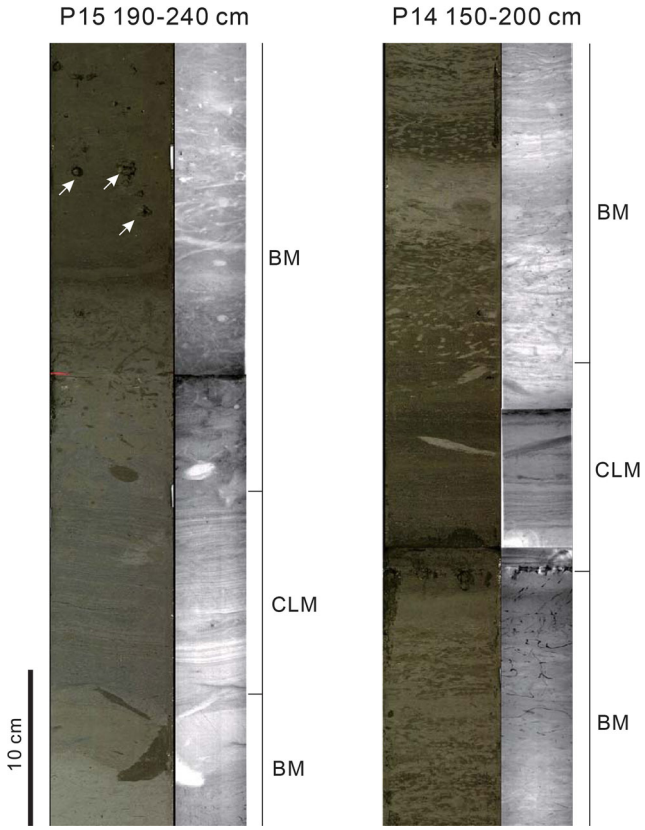

Fig. 11 Photographs and X-radiographs from selected core intervals. Sedimentary facies: *BM* bioturbated mud, *CLM* crudely laminated mud. *Arrows* Scattered pumice lapilli of U-Oki tephra layer

Preconditioning factors

Submarine failures occur in response to various major factors (Hampton et al. 1996). Sea-level fluctuations and gas charging probably have been the most important preconditioning factors in western sector of the margin of the Ulleung Basin (Fig. 16). High sedimentation rates can be ruled out for the study area because, even during sea-level lowstands, there is no direct fluvial input along the adjacent coastal zone. This is supported by the age data from sediment cores, associated with extremely low background sedimentation rates in the vicinity of the study area. Also, the N–S trending Hupo Bank on the shelf appears to act as a structural barrier for transporting sediments further to the slope regions. Indeed, this ridge has been identified as a major morphological barrier, whereby sediments from the Korean peninsula have accumulated west of the ridge since 5.5 Ma to a thickness of ca. 1 s (Hupo Basin; Yoon 1994). Hence, it is very unlikely that sedimentation rates were sufficient to build up excess pore pressure in the subsurface sediments to generate the observed slope failures.

Sea-level fluctuations and gas charging

The rapid rise and fall of the sea level over unconsolidated sediments and the effect on the stability of gas hydrates often results in submarine landslides (Maslin et al. 2004; Urlaub

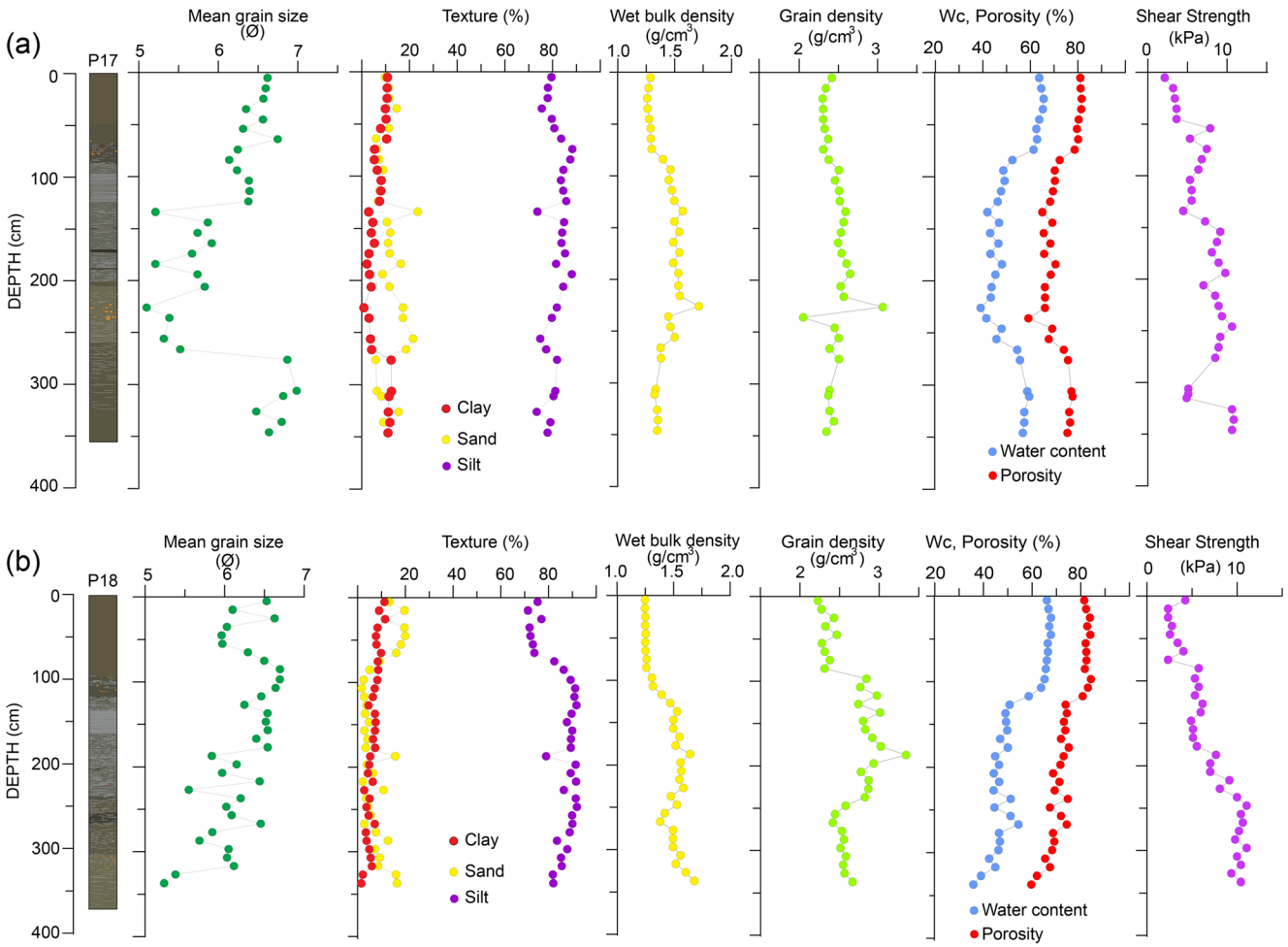

Fig. 12 Profiles of sediment texture and physical properties of cores P17 and P18. The cores are comprised largely of silt. Grain density and wet bulk density increase whereas water content decreases with increasing silt content. For core locations, see Fig. 10

et al. 2013). On the slopes, development of excess pore pressures as a result of rapid loading of sediments during sea-level falls would decrease the sediment strength and precondition the slope for failure (e.g. Stigall and Dugan 2010). An external trigger, most likely an earthquake, may then be necessary to eventually cause slope failure. Such possibility cannot be excluded in the Ulleung Basin and was previously discussed by earlier studies. Lee et al. (1996), for instance, on the basis of identified turbidites from sediment cores collected in deeper parts of the Ulleung Basin, found increased numbers of slope failures during lower sea levels in the late Pleistocene, whereas stable slope phases were found to be associated with rising sea level in the Holocene. According to Lee et al. (2010), the frequency of slope failures during eustatic lowering of sea level (~29.4–19.1 ka) is five times the frequency during the sea-level rising stage (19.1 ka–Present) on the south-western margin of the Ulleung Basin. However, as discussed above, this was most likely not the case for the western margin because the sedimentation rates were extremely low even during sea-level lowstands.

It is possible that that sea-level fall (decreasing pressure) in the late Pleistocene would cause decomposition of gas hydrates into water and methane. If these cannot readily escape, they reduce the shear strength of the sediment and thus favour slope failure (Barnes and Lewis 1991; Hovland et al. 2012). Gas hydrate dissociation was proposed for the Storegga Slide off mid-Norway (Sultan et al. 2004a) and the Blake Ridge (Dillon et al. 2001). That deep sediments of the Ulleung Basin do contain large amounts of gas hydrate and associated fluids is suggested by samples collected by the Ulleung Basin Gas Hydrate Drilling Expedition (Ryu et al. 2013) and by the occurrence of BSRs in seismic reflection data (Yoo et al. 2008; Horozal et al. 2009; Kang et al. 2009). Subbottom and sparker profiles clearly show the presence of overpressurized gases and/or gas fluids, as evidenced by the occurrence of pockmarks and seismic chimneys in upslope or adjacent areas of the scarps in the present study (Fig. 9). Pockmarks owe their origin to the upward migration

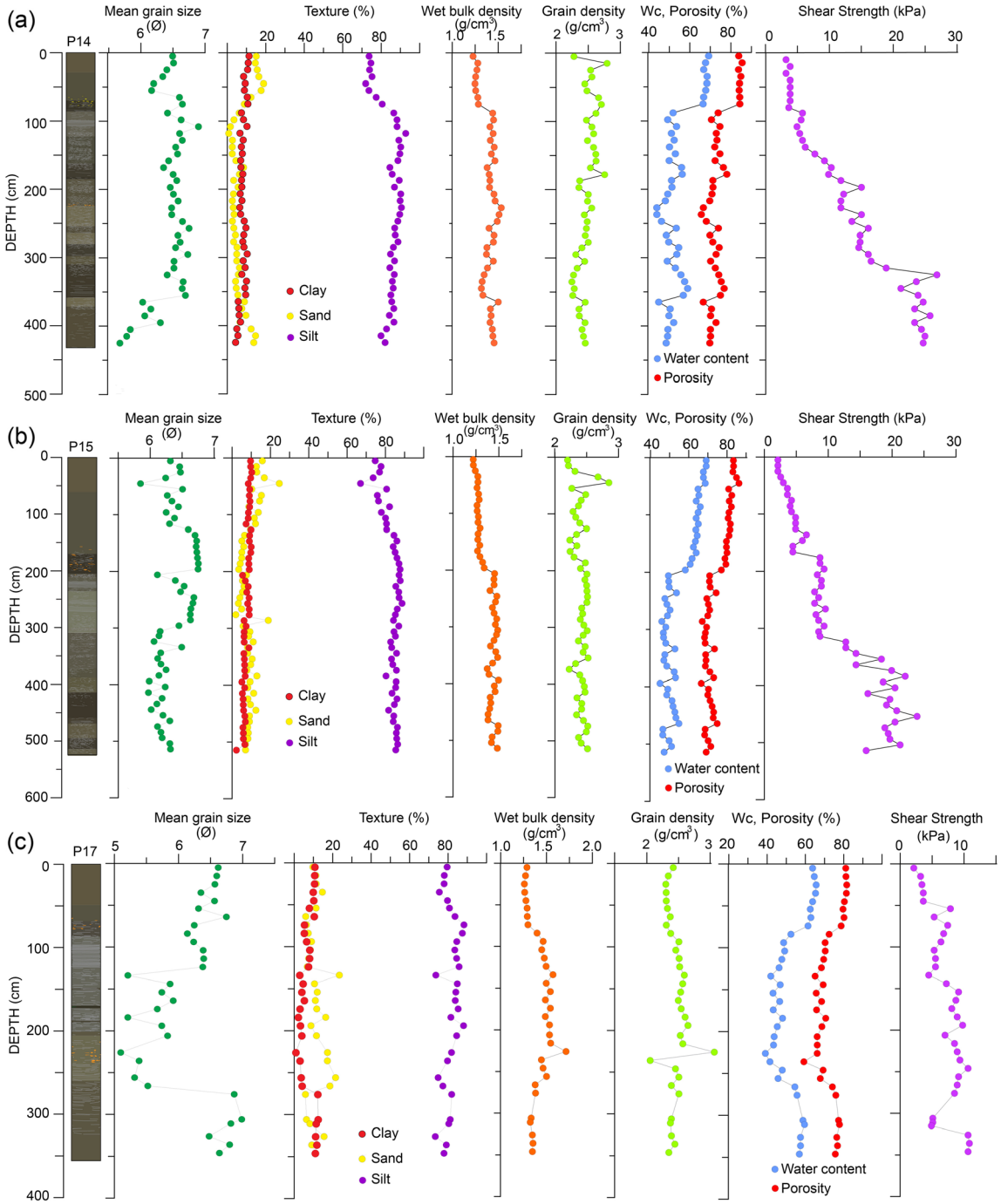

Fig. 13 Profiles of sediment texture and physical properties of cores P14, P15 and P17, located at water depths greater than 590 m and reaching peak shear strengths of 27 kPa. Note the good correlation between sediment physical properties and sediment texture. For core locations, see Fig. 10

of gas along bedding planes and cracks in subsurface sediments (Hovland et al. 2002). The presence of buried pockmarks suggests that there was gas emission in the past, which has since ceased (Fig. 9a). Pockmarks reaching the seafloor may be of the same generation as their buried counterparts, having persisted at other locations; alternatively, they may be of a younger generation. The fact that they reach the surface even though inactive at present implies that they have been active until recent times. Moreover, their identification immediately below and above the scars suggests that subsurface fluids might be playing an important role in destabilizing slope sediments. However, direct evidence for a possible link between fluid development and slope failures in the study area is not provided by this set of seismic data.

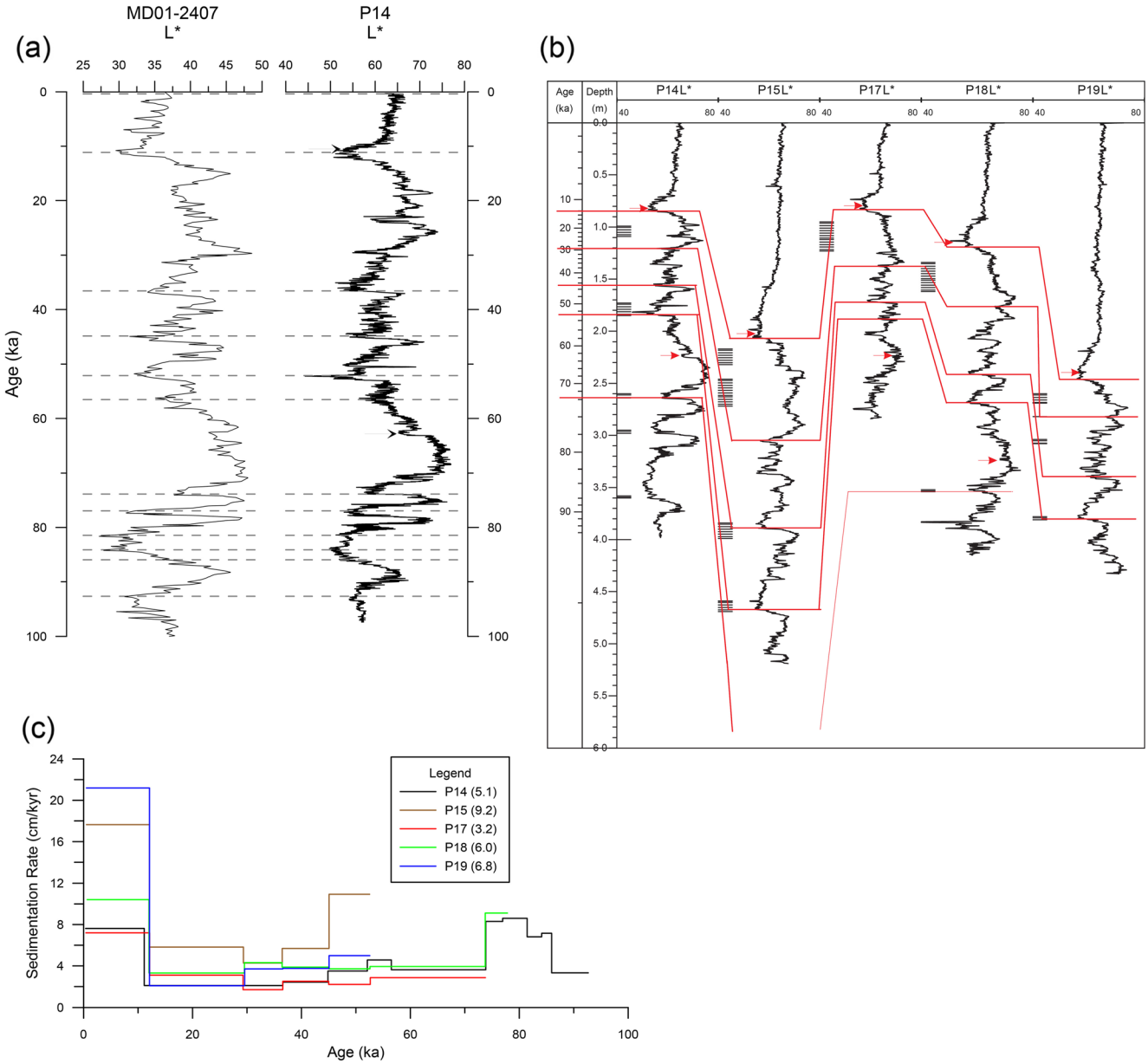

Fig. 14 **a** Correlations of L* between the MD01-2407 (Kido et al. 2007) and P14 cores (*hatched lines* tie points). Note that original P14 L* data have been converted to an age scale according to the correlation. *Upper and lower arrows* Depths of the U-Oki (10.7 ka) and SKP-II (60–61 ka) tephra layers respectively (Chun et al. 2007). **b** Correlation between the cores based on L*, tephra layers and CLM facies. *Upper and lower red arrows* Depths of the U-Oki (10.7 ka) and SKP-II (60–61 ka) tephra layers respectively (Chun et al. 2007). *Horizontal hatching* Intervals of CLM facies. *Red lines* Tie points. *Left-hand column* Age of core P14, scaled according to the depth–age conversion. **c** Sedimentation rates in the cores. Each step corresponds to a correlated interval in **b**. *Values in parentheses in legend* Average sedimentation rates in cm/1,000 years

Triggering mechanisms: earthquakes associated with tectonic activity

Several studies have revealed that mass movements are commonly triggered by earthquakes or seismic shaking associated with tectonic activity (e.g. Hampton et al. 1996; Dillon et al. 2002; Fryer et al. 2004). In this study, earthquakes are also considered as a main reason for slope failures in the working area because the East Sea region has been undergoing contractional deformation since the late Miocene (Chough and Barg 1987). The three major fault systems (Hupo, Yangsan and Ulleung) that developed in response to these tectonic events are situated in the vicinity of the study area (Fig. 17), and have been active since the Neogene (Yoon et al. 1997; Kyung 2003). Moreover, the chirp profiles clearly show that several faults offset the most recent sedimentary units immediately upslope of the scars; some extend to the seafloor, suggesting their recent activity (Figs. 5 and 8). These faults

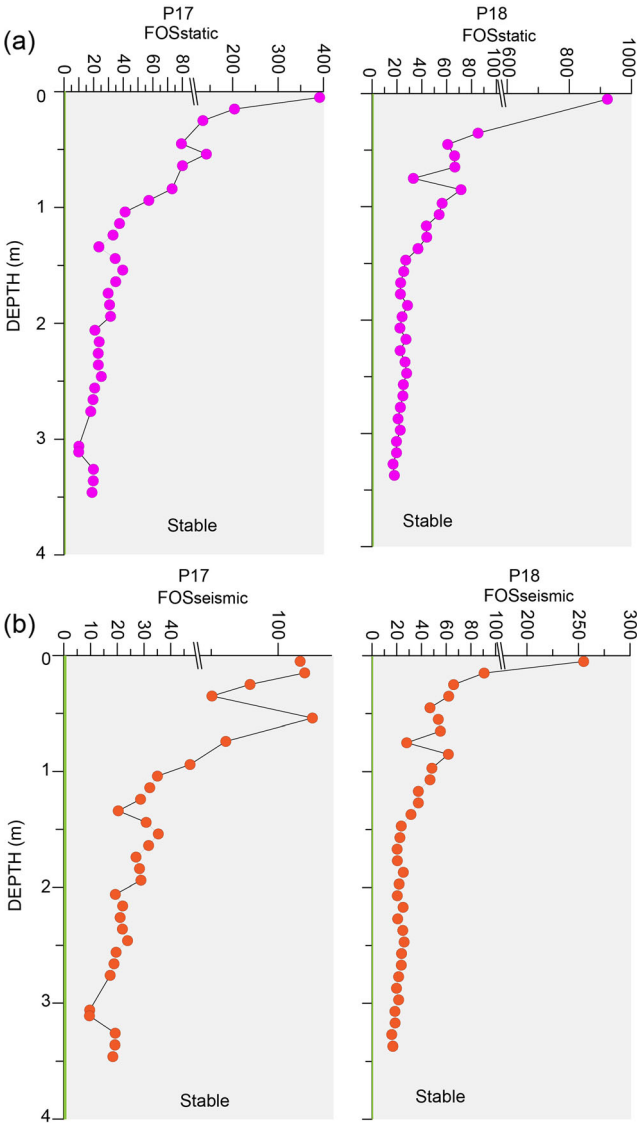

Fig. 15 Profiles of FOS_{static} (**a**) and $FOS_{seismic}$ (**b**) for cores P17 and P18. From stability analyses under static conditions even under seismic loading, the resulting factor of safety (FOS) exceeds 9 in all cases, and thus favours an exceptionally stable slope (given that FS≤1 represents slope failure)

may also be due to the retrogressive movements of sediment failure surfaces. However, the sparker profiles provide distinct evidence that they are deep seated and also visible downslope of the scarps (Fig. 5b). The presence of these faults strongly suggests that the slope has been tectonically active, even at present as well documented by the occurrence of numerous earthquakes (Fig. 17). Hence, it seems reasonable that earthquakes along the margin of the Ulleung Basin may have acted as a governing factor for weakening sediments along the slope.

Present-day slope stability

Slope failures under static conditions are generated by the overburden that imposes a shear stress in the downslope direction. Sediment failure would occur when shearing stress exceeds the shear strength of the sediments. Studies of slope stability of sediments on the southern margin of the Ulleung Basin (Chough and Lee 1987; Lee et al. 1991, 1993; Kim 1998) suggested that those slope sediments are quite stable under static undrained (rapid) loading conditions. The observed slope failures are thought to be remnants of ancient mass failures, having probably occurred during the Pleistocene lowstands of sea level when terrigenous material was more actively transported to the slope (Lee et al. 1993).

In the present study, slope stability analyses under static and seismic loading using two sediment cores suggest that the present-day slope sediments are exceptionally stable under static as well as very high seismic conditions (FOS>10). Therefore, other destabilizing processes would be necessary to trigger submarine slides at present. Some factors (e.g. high sedimentation rate) could result in greatly reduced maximum stable slopes under static loading conditions. However, as revealed by the sediment cores, the Holocene and late Pleistocene sedimentation rate in the unfailed slope areas (see cores P17 and P18 in Fig. 14c) is quite low (ca. <6 cm/1,000 years). The fact that no turbidites have yet been found within the sedimentary column in the Ulleung Basin during the Holocene (Bahk et al. 2000) supports these results.

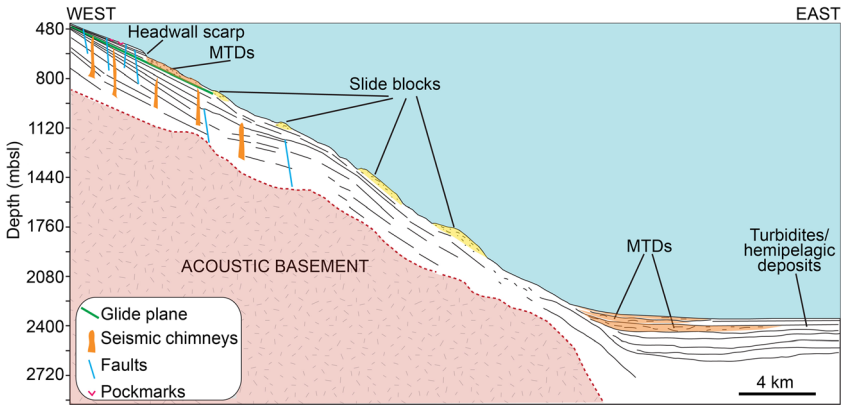

Fig. 16 East–west schematic diagram of observed submarine landslides and their corresponding deposits across the western slope of the Ulleung Basin. Note the occurrence of faults and gas-related anomalies immediately upslope of the scars

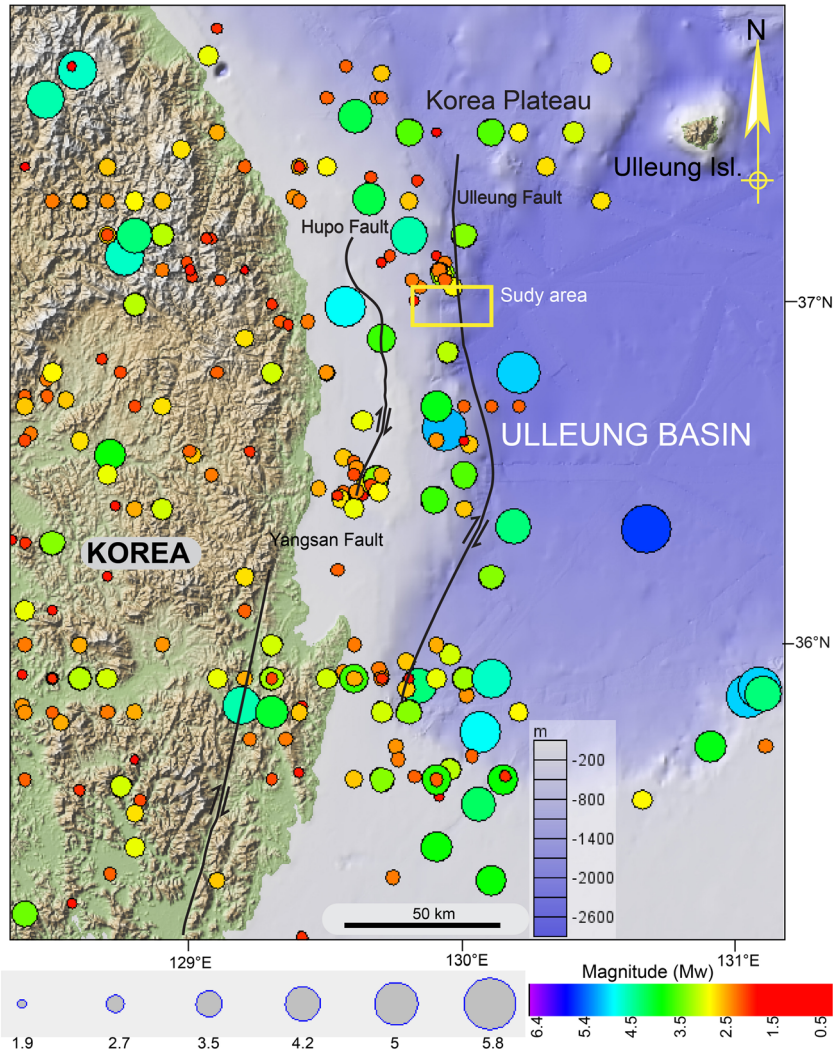

Fig. 17 Map showing the locations of earthquakes during the period 1905–2015 in the vicinity of the western continental margin of the Ulleung Basin. Earthquake data are from the Korea Meteorological Administration (2016)

For the slope failures that occurred in the past (ca. >97 ka), a state of underconsolidation with correspondingly low values of shear strength could have been present and could have led to increased instability. As stated above, it is likely that excess pore pressure caused by migrating gases lowered the shear strength of sediments in the past. Further studies (i.e. drilling glide plane), however, are necessary to verify fluid control of the formation of these submarine landslides and the nature of the slip surfaces.

Conclusions

Based on analyses of multibeam bathymetric data as well as sparker profiles, subbottom chirp profiles and sediment cores, the present study provides novel evidence of submarine landslides on the western slope of the Ulleung Basin. Submarine failures are extremely well documented by the occurrence of headwall scarps and by the presence of major seismic facies of landslide deposits that are recorded in the sedimentary column as transparent to chaotically reflecting layers. At least seven submarine failures have occurred. The observed slides appear to be the result of retrogressive-type failure.

The submarine failures left distinct headwall scarps on the upper slope, and various slide blocks formed on the middle and lower slopes. Headwall scars have heights of up to 60 m and occur in water depths of ~600 m. The landslides have volumes in the range of 6 km^3, cover a seafloor area of 120 km^2 and have run-out distances of up to 30 km. They are small compared to those along the southern slope, plausibly due to low sedimentation rates. The probable ages of the slides vary but all are older than 97 ka.

Gas charging appears to be the major preconditioning factor, most likely aided by earthquakes associated with tectonic activity. Although major sediment failures occurred in the past, the present-day slope sediments appear to be quite stable (factor of safety well beyond 1) under static and even seismic conditions. Hence, additional forces such as excess pore pressure caused by fluids would be necessary to initiate landslides in this area.

Acknowledgements This work was supported by the Marine Geological and Geophysical Mapping of the Korean Seas Project (16–3317) and partly by basic research project "Study on marine geology and mineral resources in buried paleochannel of Seomjin River, South Sea (16–3316) of the Korea Institute of Geoscience and Mineral Resources (KIGAM). We thank A. Micallef, A. Georgiopoulou and the journal editors for their constructive comments. We also thank the crew of R/V Tamhae II for their assistance during data acquisition.

Compliance with ethical standards

Conflict of interest The authors declare that there is no conflict of interest with third parties.

References

Bae SW, Lee KE, Park Y, Kimoto K, Ikehara K, Harada N (2014) Sea surface temperature and salinity changes near the Soya Strait during the last 19 ka. Quat Int 344:200–210

Bahk JJ, Chough SK, Han SJ (2000) Origins and paleoceanographic significance of laminated muds from the Ulleung Basin, East Sea (Sea of Japan). Mar Geol 162:459–477

Baraza J, Ercilla G, Lee H (1992) Geotechnical properties and preliminary assessment of sediment stability on the continental slope of the Northwestern Alboran Sea. Geo-Mar Lett 12:150–156

Barnes PM, Lewis KB (1991) Sheet slides and rotational failures on a convergent margin: the Kidnappers Slide, New Zealand. Sedimentology 38:205–221

Blum P (1997) Physical properties handbook: a guide to the shipboard measurement of physical properties of deep-sea cores. ODP Tech Note 26

Bondevik S, Lovholt F, Harbitz CB, Mangerud J, Dawson A, Svendsen JI (2005) The Storegga Slide tsunami; comparing field observations with numerical simulations. Mar Petrol Geol 22:195–208

Camerlenghi A, Urgeles R, Ercilla G, Brückman W (2007) Scientific ocean drilling behind the assessment of geo-hazards from submarine slides. Sci Drill 4:45–47

Chough SK (1983) Marine geology of Korean seas. Dordrecht, Boston

Chough SK, Barg E (1987) Tectonic history of Ulleung basin margin, East Sea (Sea of Japan). Geology 15:45–48

Chough SK, Lee HJ (1987) Stability of sediments on the Ulleung basin slope. Mar Geotechnol 17:123–132

Chough SK, Jeong KS, Honza E (1985) Zoned facies of mass-flow deposits in the Ulleung (Tsushima) Basin, East Sea (Sea of Japan). Mar Geol 65:113–125

Chough SK, Yoon SH, Lee HJ (1991) Submarine slides in the eastern continental margin, Korea. Mar Geotechnol 10:71–82

Chun JH, Cheong D, Ikehara K, Han SJ (2007) Age of the SKP-I and SKP-II tephras from the southern East Sea/Japan Sea: implications for interstadial events recorded in sediment from marine isotope stages 3 and 4. Palaeogeogr Palaeoclimatol Palaeoecol 1–2:100–114

Dan G, Sultan N, Savoye B (2007) The 1979 Nice harbour catastrophe revisited: trigger mechanism inferred from geotechnical measurements and numerical modeling. Mar Geol 245:40–64

Dillon WP, Nealon JW, Taylor MH, Lee MW, Drury RM, Anton CH (2001) Seafloor collapse and methane venting associated with gas hydrate on the Blake Ridge—causes and implications to seafloor stability and methane release. In: Paull CK, Dillon WP (eds) Natural gas hydrates: Occurrence, distribution, and detection. Geophys Monogr Ser 124:211–233

Dillon WP, Risch JS, Scanlon KM, Valentine PC, Huggert QC (2002) Ancient crustal fractures control the location and size of collapsed blocks at the Blake Escarpment, east of Florida. In: Schwab WC, Lee HJ, Twichell DC (eds) Submarine landslides: Selected studies in the U.S. Exclusive Economic Zone. US Geol Surv Bull 54–59:1993

Fryer GJ, Watts P, Pratson LF (2004) Source of the great tsunami of 1 April 1946: a landslide in the upper Aleutian forearc. Mar Geol 203: 201–218

Hampton MA, Lee HJ, Locat J (1996) Submarine landslides. Rev Geophys 34:33–59

Horozal S, Lee GH, Yi Y, Yoo DG, Park KP, Lee HY, Kim W, Kim HJ, Lee K (2009) Seismic indicators of gas hydrate and associated gas in the Ulleung Basin, East Sea (Japan Sea) and implications of heat flows derived from depths of the bottom-simulating reflector. Mar Geol 258:126–138

Horozal S, Bahk JJ, Lee SH, Urgeles R, Kim SP, Kim GY, Cukur D, Lee GH, Ryu BJ, Kim JH (2016) Late Neogene–Quaternary submarine mass wasting along the margins of the Ulleung Basin, East Sea: geomorphologic controls and geohazard potential. Quat Int 392: 69–98. doi:10.1016/j.quaint.2015.06.056

Hovland M, Gardner JV, Judd AG (2002) The significance of pockmarks to understanding fluid flow processes and geohazards. Geofluids 2: 127–136

Hovland M, Jensen S, Fichler C (2012) Methane and minor oil macroseep systems – their complexity and environmental significance. Mar Geol 332–334:163–173

Hustoft S, Bünz S, Mienert J (2010) Three-dimensional seismic analysis of the morphology and spatial distribution of chimneys beneath the Nyegga pockmark field, offshore mid-Norway. Basin Res 22:465–480

Hutton EW, Syvitski JP (2004) Advances in the numerical modeling of sediment failure during the development of a continental margin. Mar Geol 23:367–380

Ingle JC (1975) Pleistocene and Pliocene foraminifera from the Sea of Japan, Leg 31, Deep Sea Drilling Project. Initial Rep Deep Sea Drill Proj 31:693–701

Kang DH, Yoo DG, Bahk JJ, Koo NH, Kim WS, Park KS, Park KP, Kim JS (2009) The occurrence patterns of gas hydrate in the Ulleung Basin, East Sea. J Geol Soc Korea 45:143–155

Kayen R, Lee H (1991) Pleistocene slope instability of gas hydrate-laden sediment on the Beaufort sea margin. Mar Geotechnol 10:125–141

Khim BK, Park YH, Bahk JJ, Jin JH, Lee GH (2008) Spatial and temporal variation of geochemical properties and paleoceanographic implications in the South Korea Plateau (East Sea) during the late Quaternary. Quat Int 176–177:46–61

Kido Y, Minami I, Tada R, Fujine K, Irino T, Ikehara K, Chun JH (2007) Orbital-scale stratigraphy and high-resolution analysis of biogenic components and deep water oxygenation conditions in the Japan Sea during the last 640 kyrs using XRF microscanner. Palaeogeogr Palaeoclimatol Palaeoecol 247:32–49

Kim GY (1998) Geotechnical property and paleoceanographic characteristics of the late Quaternary Ulleung Basin sediment, the East Sea, Korea. Dissertation, Pukyong National University

Koo BY, Kim SP, Lee GS, Chung GS (2014) Seafloor morphology and surface sediment distribution of the southwestern part of the Ulleung Basin, East Sea. J Korean Sci Soc 35(2):131–146

Korea Meteorological Administration (2016) The distribution map of the epicenter (in Korean). http://www.kma.go.kr/weather/earthquake/domestictrend.jsp

Krastel S, Wynn RB, Hanebuth TJJ, Henrich R, Holz C, Meggers H, Kuhlmann H, Georgiopoulou A, Schulz HD (2006) Mapping of seabed morphology and shallow sediment structure of the Mauritania continental margin, Northwest Africa: some implications for geohazard potential. Norw J Geol 86:163–176

Krastel S, Wynn RB, Georgiopoulou A, Geersen J, Henrich R, Meyer M, Schwenk T (2012) Large scale mass wasting at the NW-African Continental Margin: some general implications for mass wasting at passive continental margins. In: Yamada Y, Kawamura K, Ikehara

K, Ogawa Y, Urgeles R, Mosher D, Chaytor J, Strasser M (eds) Submarine mass movements and their consequences, vol 31, Advances in Natural and Technological Hazards Research. Springer, Heidelberg, pp 189–199

Kyung JB (2003) Paleoseismology of the Yangsan fault, southeastern part of the Korean peninsula. Ann Geophys 46:983–996

Lee GH, Suk BC (1998) Latest Neogene-Quaternary seismic stratigraphy of the Ulleung Basin, East Sea (Sea of Japan). Mar Geol 146:205–224

Lee HJ, Chough SK, Chun SS, Han SJ (1991) Sediment failure on the Korea Plateau slope, East Sea (Sea of Japan). Mar Geol 97:363–377

Lee HJ, Chun SS, Yoon SH, Kim SR (1993) Slope stability and geotechnical properties of sediment of the southern margin of Ulleung Basin, East Sea (Sea of Japan). Mar Geol 110:31–45

Lee HJ, Chough SK, Yoon SH (1996) Slope-stability change from late Pleistocene to Holocene in the Ulleung Basin, East Sea (Japan Sea). Sediment Geol 104:39–51

Lee SH, Chough SK, Back GG, Kim YB, Sung BS (1999) Gradual downslope change in high-resolution acoustic characters and geometry of large-scale submarine debris lobes in Ulleung Basin, East Sea (Sea of Japan), Korea. Geo-Mar Lett 19(4):254–161. doi:10.1007/s003670050116

Lee SH, Bahk JJ, Kim HJ, Lee KE, Jou HT, Suk BC (2010) Changes in the frequency, scale, and failing areas of latest Quaternary (<29.4 cal. ka B.P.) slope failures along the SW Ulleung Basin, East Sea (Japan Sea), inferred from depositional characters of densely dated turbidite successions. Geo-Mar Lett 30:133–142. doi:10.1007/s00367-009-0168-0

Leynaud D, Mienert J, Vanneste M (2009) Submarine mass movements on glaciated and non-glaciated European continental margins: a review of triggering mechanisms and preconditions to failure. Mar Petrol Geol 26:618–632

Locat J, Lee HJ (2002) Submarine landslides: advances and challenges. Can Geotech J 39:193–212

Maslin M, Owen M, Day S, Long D (2004) Linking continental-slope failures and climate change: testing the clathrate gun hypothesis. Geology 32:53–56

Masson DG, Harbitz CB, Wynn RB, Pedersen G, Lovholt F (2006) Submarine landslides: processes, triggers and hazard prediction. Philos Trans R Soc A 364:2009–2039

Mienert J, Vanneste M, Bünz S, Andreassen K, Haflidason H, Sejrup HP (2005) Ocean warming and gas hydrate stability on the mid-Norwegian margin at the Storegga Slide. Mar Petrol Geol 22:233–244

Morgenstern NR (1967) Submarine slumping and the initiation of turbidity currents. In: Richards AF (ed) Marine geotechnique. University of Illinois Press, Urbana, pp 189–220

Morgenstern NR, Price VE (1965) The analysis of the stability of general slip surfaces. Géotechnique 15(1):79–93

Mosher DC, Moscardelli L, Shipp RC, Chaytor JD, Baxter CDP, Lee HJ, Urgeles R (2010) Submarine mass movements and their consequences. In: Mosher DC, Shipp C, Moscardelli L, Chaytor J, Baxter C, Lee H, Urgeles R (eds) Submarine mass movements and their consequences. Advances in Natural and Technological Hazards Research, vol 28. Springer, Heidelberg, pp 1–8

Newton CS, Shipp RC, Mosher DC (2004) Importance of mass transport complexes in the Quaternry development of the Nile Fan, Egypt. Offshore Technology conference paper, Houston, **no 16742**

Nixon MF, Grozic JLH (2007) Submarine slope failure due to gas hydrate dissociation: a preliminary quantification. Can Geotech J 44:314–325

Park YJ, Kang NK, Yi BY, Yoo DG (2015) Origin and distribution of cut and fill structures in the southwestern margin of Ulleung Basin, East Sea. Geophys Geophys Explor 18:39–53

Ryu BJ, Kim GY, Chun JH, Bahk JJ, Lee JY, Kim JH, Yoo DG, Collett TS, Riedel M, Torres ME, Lee SR (2013) The scientific results of the Second Gas Hydrate Drilling Expedition in the Ulleung Basin (UBGH2). Mar Petrol Geol 47:1–20

Shanmugam G (2009) Slides, slumps, debris flows, and turbidity currents. In: Steele JH, Thorpe SA, Turekian KK (eds) Encyclopedia of Ocean Sciences, 2nd edn. Academic Press, Waltham, pp 447–467

Shipp C, Nott JA, Newlin JA (2004) Physical characteristics and impact of mass transport complexes on deepwater jetted conductors and suction anchor piles. Offshore Technology conference, Houston

Stigall J, Dugan B (2010) Overpressure and earthquake initiated slope failure in the Ursa region, northern Gulf of Mexico. J Geophys Res 115, B04101. doi:10.1029/2009JB006848

Strozyk F, Strasser M, Krastel S, Meyer M, Huhn K (2010) Reconstruction of retreating mass wasting in response to progressive slope steepening of the northeastern Cretan margin, eastern Mediterranean. Mar Geol 271:44–54

Sultan N, Cochonat P, Foucher JP, Mienert J (2004a) Effect of gas hydrates melting on seafloor slope instability. Mar Geol 213(1–4):379–401

Sultan N, Cochonat P, Canals M, Cattaneo A, Dennielou B, Haliffladson H, Laberg JS, Long D, Mienert J, Trincardi F (2004b) Triggering mechanisms of slope instability processes and sediment failure on continental margins: a geotechnical approach. Mar Geol 213:291–321

Tappin DR, Watts P, McMurtry GM, Lafoy Y, Matsumoto T (2001) The Sissano Papua New Guinea tsunami of July 1998 - offshore evidence on the source mechanism. Mar Geol 175:1–23

ten Brink US, Lee HJ, Geist EL, Twichell D (2009) Assessment of tsunami hazard to the U.S. East Coast using relationships between submarine landslides and earthquakes. Mar Geol 264:65–73

Urgeles R, Camerlenghi A (2013) Submarine landslides of the Mediterranean Sea: trigger mechanisms, dynamics and frequency-magnitude distribution. J Geophys Res Earth Surf 118:2600–2618

Urlaub M, Talling PJ, Masson DG (2013) Timing and frequency of large submarine landslides: implications for understanding triggers and future geohazard. Quat Sci Rev 72:63–82

Völker D, Scholz F, Geersen J (2011) Analysis of submarine landsliding in the rupture area of the 27 February 2010 Maule earthquake, Central Chile. Mar Geol 288:79–89

Yamada Y, Kawamura K, Ikehara K, Ogawa Y, Urgeles R, Mosher D, Chaytor J, Strasser M (2012) Submarine mass movements and their consequences. In: Yamada Y, Kawamura K, Ikehara K, Ogawa Y, Urgeles R, Mosher D, Chaytor J, Strasser M (eds) Submarine mass movements and their consequences, vol 31, Advances in Natural and Technological Hazards Research. Springer, Heidelberg, pp 1–12

Yoo DG, Kang DH, Koo NH, Kim WS, Kim GY, Kim BY, Chung SH, Kim YJ, Lee HY, Park KP, Lee GH, Park SC (2008) Geophysical evidence for the occurrence of gas hydrate in the Ulleung Basin, East Sea. J Geol Soc Korea 44:645–655

Yoon SH (1994) The eastern continental margin of Korea. Seismic stratigraphy, geologic structure and tectonic evolution. Dissertation, Seoul National University

Yoon SH, Park SJ, Chough SK (1997) Western boundary fault systems of Ulleung Back-arc Basin: further evidence of pull-apart opening. Geosci J 1(2):75–88